COROTATING STRUCTURE IN THE SOLAR WIND

R. L. CAROVILLANO
Dept. of Physics, Boston College, Chestnut Hill, Mass., U.S.A.
and
G. L. SISCOE
Dept. of Meteorology, University of California, Los Angeles, Calif., U.S.A.

(Received 18 February, 1969)

Abstract. The hydrodynamic equations which describe the radial solar wind expansion are linearized and specialized to treat corotating perturbations. Approximate solutions are found which are time stationary in the corotating reference frame. The solutions predict the behavior of corotating structures for a given boundary condition close to the sun. In particular, the structure resulting from the interaction of fast and slow streams is described. Comparison with sector structure data shows reasonable qualitative and quantitative agreement.

1. Introduction

This paper presents the initial results of a theoretical study of the role solar rotation plays in determining solar wind structure. The approach is to perturb the spherically symmetric hydrodynamic solution of the solar wind problem on a boundary fairly close to the sun. Corotating perturbations are used to represent the effects of stationary features on the solar surface such as hot regions and cool regions. Solutions of the perturbation equations are sought which are time stationary in the corotating frame of reference. Thus, the results describe time stationary corotating features in the solar wind produced by inhomogeneities in the solar atmosphere.

For the purpose of exposing the method and gaining insight into the relevant physical processes, we limit the discussion to approximate solutions. This restricts the validity to the region of space between approximately 0.1 AU and 1 AU and to large scale features, namely, large enough to require at least 2.5 days to rotate passed a fixed point. The present solutions applied to the corotating sector structure observed by IMP-1 gives reasonable agreement between observed and predicted behavior. Subsequent articles will discuss numerical solutions of wider validity and the effects of a magnetic field.

The solution treated in greatest detail describes the interaction between corotating fast and slow streams. This case is represented by the following inner boundary condition: zero density perturbation, zero azimuthal velocity perturbation, but non-zero radial velocity perturbation. The solutions describe the radial growth of the density and azimuthal velocity perturbations and the radial change in the radial velocity perturbation. Thus, we can predict the resulting structure in these parameters at the orbit of earth. The predictions agree with qualitative ideas previously expressed in the literature. The compression and rarefaction produced by corotating irregularities

have been described qualitatively by Parker (1965). The piling up of the density on the leading edge of a fast stream was suggested by Neugebauer and Snyder (1967) to explain observed features in the Mariner 2 plasma data. The decrease in density at the trailing edge of a fast stream was postulated by Sarabhai (1963). The azimuthal deflections resulting from a fast stream pushing against a slow stream along a spiral interface was suggested by Dessler (1967). The present solutions allow quantitative estimates of these effects.

2. Mathematical Treatment and Results

We will use a heliocentric spherical polar coordinate system with the polar axis along the sun's axis of rotation. At the north pole $\theta=0$, and the angle φ increases in the direction the sun rotates.

LINEARIZED EQUATIONS

The equations determining the flow are Euler's equation and the continuity equation:

$$\frac{\partial \mathbf{V}}{\partial t} + (\mathbf{V}\cdot\nabla)\,\mathbf{V} + \frac{\nabla p}{\varrho} = -\nabla\Phi \tag{1}$$

$$\frac{\partial \varrho}{\partial t} + \nabla\cdot(\varrho\mathbf{V}) = 0 \tag{2}$$

where $\mathbf{V}$ is the velocity, p the thermal pressure, ϱ the density, and Φ the gravitational potential. We assume the pressure and density are related by a polytropic law:

$$p = \alpha\varrho^{\gamma} \tag{3}$$

where the proportionality constant α and the polytropic index γ will be held constant throughout the calculation.

Each variable is split into a zero order part and a perturbation. The zero order term is the solution of the time independent, spherically symmetric problem familiar from the work of Parker (see, for example, Parker, 1963)

$$(\mathbf{V}_0\cdot\nabla)\,\mathbf{V}_0 + \frac{\nabla p_0}{\varrho_0} = -\nabla\Phi \tag{4}$$

$$\nabla\cdot(\varrho_0\mathbf{V}_0) = 0 \tag{5}$$

$$p_0 = \alpha\varrho_0^{\gamma}. \tag{6}$$

By the assumption of spherical symmetry $\mathbf{V}_0 = V_0(r)\,\hat{r}$, where $\hat{r}$ is a unit vector in the radial direction.

We confine the treatment of the perturbations to the equatorial plane ($\theta=\pi/2$), and we assume the perturbations to be north-south symmetric so that $\partial/\partial\theta=0$ at $\theta=\pi/2$. We also ignore the divergence in the θ-direction for this first analysis. This can be taken either as an approximation or as a special latitudinal boundary condition. The linearized equations for the perturbations in the equatorial plane can then be written

in the form

$$\left(\frac{\partial}{\partial r}+\frac{1}{V_0}\frac{\partial}{\partial t}\right)(V_0 V_{1r})+\frac{\partial}{\partial r}\left(c_s^2\frac{\varrho_1}{\varrho_0}\right)=0 \tag{7}$$

$$\left(\frac{\partial}{\partial r}+\frac{1}{V_0}\frac{\partial}{\partial t}\right)(rV_{1\varphi})+\frac{c_s^2}{V_0}\frac{\partial}{\partial\varphi}\left(\frac{\varrho_1}{\varrho_0}\right)=0 \tag{8}$$

$$\left(\frac{\partial}{\partial r}+\frac{1}{V_0}\frac{\partial}{\partial t}\right)\left(\frac{\varrho_1}{\varrho_0}\right)+\frac{\partial}{\partial r}\left(\frac{V_{1r}}{V_0}\right)+\frac{1}{rV_0}\frac{\partial V_{1\varphi}}{\partial\varphi}=0 \tag{9}$$

where V_{1r} and $V_{1\varphi}$ are the r and φ components of the perturbation velocity ($V_{1\theta}=0$ by the assumption of north-south symmetry), and $c_s^2=\alpha\varrho_0^{\gamma-1}$ is the zero order sound speed. Equations (7) and (8) derive from the r and φ components respectively of Euler's equation, and Eq. (9) derives from the continuity equation.

CO-ROTATING PERTURBATIONS

As explained earlier, we are interested in perturbations that co-rotate with the sun. Thus, in the frame of reference rotating with the sun (more precisely, rotating with the solar equator) the perturbations depend only on the spatial variables and not on time. Therefore, in an inertial frame of reference, the variables φ and t are not independent but must always occur in the form $\varphi-\Omega t$, where Ω is the angular velocity of the sun. Let

$$\eta=\varphi-\Omega t. \tag{10}$$

Then in the equatorial plane, the perturbation variables are functions of r and η only. Eqs. (7), (8), and (9) now become

$$\left(\frac{\partial}{\partial r}-\frac{\Omega}{V_0}\frac{\partial}{\partial\eta}\right)(V_0 V_{1r})+\frac{\partial}{\partial r}\left(c_s^2\frac{\varrho_1}{\varrho_0}\right)=0 \tag{11}$$

$$\left(\frac{\partial}{\partial r}-\frac{\Omega}{V_0}\frac{\partial}{\partial\eta}\right)(rV_{1\varphi})+\frac{c_s^2}{V_0}\frac{\partial}{\partial\eta}\left(\frac{\varrho_1}{\varrho_0}\right)=0 \tag{12}$$

$$\left(\frac{\partial}{\partial r}-\frac{\Omega}{V_0}\frac{\partial}{\partial\eta}\right)\left(\frac{\varrho_1}{\varrho_0}\right)+\frac{\partial}{\partial r}\left(\frac{V_{1r}}{V_0}\right)+\frac{1}{rV_0}\frac{\partial V_{1\varphi}}{\partial\eta}=0. \tag{13}$$

TWO INTEGRALS OF MOTION

The three equations can be manipulated to yield two integrals of the motion analogous to the vorticity integral and the Bernoulli integral. For this purpose, notice that any function of the variable ξ defined by

$$\xi=\Omega\int\frac{\mathrm{d}r}{V_0}+\eta \tag{14}$$

is annihilated by the operator $\partial/\partial r-(\Omega/V_0)\,\partial/\partial\eta$, which occurs in all three equations. That is,

$$\left(\frac{\partial}{\partial r}-\frac{\Omega}{V_0}\frac{\partial}{\partial\eta}\right)F(\xi)=0, \tag{15}$$

where F is an arbitrary function. Operating on Eq. (11) with $\partial/\partial\eta$ and on Eq. (12) with $(\partial/\partial r)\, V_0$, subtracting and using Eq. (15), we find

$$\frac{\partial V_{1r}}{\partial \eta} - \frac{\partial r V_{1\varphi}}{\partial r} = \frac{G(\xi)}{V_0} \tag{16}$$

where G is an arbitrary function. Let $\omega = (\nabla \times \mathbf{V})_\theta$ be the vorticity (note that $\nabla \times \mathbf{V}$ has only a θ-component in the equatorial plane). Then the left hand side of equation (16) is just $r\omega$. Eq. (16) states that $r\omega V_0$ is a constant on lines of constant ξ, which are co-rotating spirals as can be seen from equation (14). In the case $V_0 = \text{constant}$, the spirals are the familiar Archimedes spirals.

The second integral of motion is found by subtracting Ω times Eq. (12) from Eq. (11) and using Eq. (15):

$$V_0 V_{1r} - \Omega r V_{1\varphi} + c_s^2 \frac{\varrho_1}{\varrho_0} = F(\xi). \tag{17}$$

Here F is an arbitrary function.

APPROXIMATE SOLUTIONS

The general zero order solutions are algebraically complicated so that exact general solutions of the perturbation equations are difficult to find. However, the exact zero order solutions are well approximated by simple functions with which the perturbation equations can be solved. In effect, each zero order function can be split into a simple function plus a small correction term. Since the zero order terms multiply first order terms in the perturbation equations, the correction terms can be dropped without significant loss of accuracy.

Approximate zero order solutions that apply to the region of space roughly between 0.1 AU and 1 AU are

$$V_0 = \text{constant} \tag{18}$$

$$\varrho_0 = \varrho_a \frac{a^2}{r^2} \tag{19}$$

where ϱ_a is the density at $r = a$. We set $r = a$ at the inner boundary of the region where the approximation used here is valid. We assume $a = 0.1$ AU to be reasonable for the inner boundary. A second approximation taken to be valid in the range $0.1\ \text{AU} < r < 1\ \text{AU}$ is

$$c_s^2 = \text{constant}. \tag{20}$$

Eq. (20) holds exactly for the case $\gamma = 1$ which corresponds to an isothermal extended solar atmosphere. There is experimental evidence that in the region under discussion γ might lie in the range 1.2 to 1.4 all of the time for the electron component and part of the time for the proton component (Strong *et al.*, 1966; Montgomery *et al.*, 1968). The isothermal approximation $\gamma = 1$, therefore, seems reasonable in this single fluid treatment of the problem. For comparison, the case $\gamma = \frac{3}{2}$ is treated in Appendix A.

With these approximations the perturbation equations are much simpler. To aid solving them, we introduce the dimensionless variables s, $x(s)$, $y(s)$, and $z(s)$ defined

by

$$s = r/a \tag{21}$$

$$\frac{V_{1r}}{V_0} = x(s)\, e^{ik\xi} \tag{22}$$

$$s\frac{V_{1\varphi}}{V_0} = y(s)\, e^{ik\xi} \tag{23}$$

$$\frac{\varrho_1}{\varrho_0} = z(s)\, e^{ik\xi} \tag{24}$$

where now

$$\xi = \varepsilon s + \eta \tag{25}$$

with

$$\varepsilon = \frac{a\Omega}{V_0}. \tag{26}$$

In these definitions, k is an integer in order that the η dependence of the perturbations be single valued. Since the equations are linear, the general solution is obtained by superposing solutions with different k. The variables x, y, and z give the relative amplitudes and phases as a function of radial distance of the perturbations V_{1r}, $V_{1\varphi}$, and ϱ_1 on lines of constant ξ, which in the present approximation are rotating Archimedes spirals.

Introducing the above definitions into the three independent Eqs. (12), (13), and (17) yields, respectively

$$y' + \frac{ik}{M_s^2}\, z = 0 \tag{27}$$

$$x' + ik\varepsilon x + \frac{ik}{s^2}\, y + z' = 0 \tag{28}$$

$$x - \varepsilon y + \frac{z}{M_s^2} = f \tag{29}$$

where

$$M_s = \frac{V_0}{c_s}. \tag{30}$$

The constant f is defined by

$$F(\xi) = V_0^2 f\, e^{ik\xi} \tag{31}$$

and primes denote differentiation with respect to s. The three equations can be manipulated to give a single equation for y:

$$(M_s^2 - 1)\, y'' - 2ik\varepsilon y' + k^2\left(\frac{1}{s^2} + \varepsilon^2\right) y = -k^2 \varepsilon f\,. \tag{32}$$

The general solution of this equation is among the 'higher' functions and little is

learned by writing it down. Physical insight is gained from an approximate solution valid for the case of primary interest here. To arrive at the approximation, it is useful to note typical values of the terms entering the equation. Experimentally one finds M_s^2 in the range 10 to 10^2, ε is about 10^{-1} for $V_0 = 400$ km/sec, and s varies from 1 to 10. For these values, if we restrict our attention to the case $k \leqslant M_s$ and the boundary condition

$$y(1) = z(1) = 0, \qquad x(1) \neq 0 \tag{33}$$

a simple approximate solution to Eq. (32) can be obtained.

The condition on k restricts the validity of the result to large scale features. For example, the case $k=4$ corresponds to 4 velocity maxima and 4 minima in one solar rotation, and it, therefore, represents roughly the quadrupole sector structure observed during the last solar minimum (Wilcox and Ness, 1965). The result to be given here should be valid for $k<10$. (The solutions valid for larger values of k grow very rapidly with s and the linear approximation is probably no good at $s=10$(1 AU).)

The boundary condition (33) corresponds to zero perturbation in the density and the azimuthal velocity at the inner boundary but a non-zero perturbation in the radial velocity. The solution will describe the growth of the density and azimuthal velocity perturbations which results when different velocity streams are caused to interact by the rotation of the sun. For completeness, approximate solutions valid for other boundary conditions are derived in Appendix B. The boundary condition (33) together with Eqs. (27) and (29) implies

$$y'(1) = 0 \tag{34}$$

$$x'(1) = f. \tag{35}$$

It can now be seen that for the present case Eq. (32) is well approximated simply by

$$M_s^2 y'' = -k^2 \varepsilon f. \tag{36}$$

Although the coefficient of y in Eq. (32) is possibly as large as that of y'' for $s=1$, both y and y' are zero there; hence, y remains small until s is fairly large and then the y coefficient is small. The solution of Eq. (36) consistent with the boundary conditions is

$$y = -\frac{k^2 \varepsilon}{2M_s^2}(s-1)^2 x(1). \tag{37}$$

From Eqs. (27) and (29) we then find

$$z = -ik\varepsilon(s-1)x(1) \tag{38}$$

$$x = \left[1 + \frac{ik\varepsilon}{M_s^2}(s-1) - \frac{k^2\varepsilon}{2M_s^2}(s-1)^2\right]x(1). \tag{39}$$

To get a feeling for the error present in this solution, let $M_s=10$ and $k=4$. For these values, the maximum ratio of the terms dropped in Eq. (32) to those kept is less than 0.1. The error increases for smaller M_s and for larger k.

3. Interpretation of Results

The solutions reveal that both ϱ_1 and $V_{1\varphi}$ grow from zero essentially linearly with distance away from the inner boundary (recall $V_{1\varphi} \propto y/s$). In a sense these quantities are unstable with respect to perturbations in the radial velocity. The 'instability' is driven by the rotation of the sun; however, it does not remove energy from the solar rotation. The energy is merely redistributed, which reduces the perturbation in the radial velocity as can be seen from Eq. (39).

Consider the relative amplitudes and phases at $s = 10$. If we ignore the imaginary part of x which is smaller compared to the other terms in the range of interest, we find

$$\left|\frac{V_{1\varphi}}{V_{1r}}\right|_{s=10} = \frac{0{\cdot}4k^2/M_s^2}{1 - 0{\cdot}4k^2/M_s^2} \tag{40}$$

$$\left|\frac{\varrho_1}{\varrho_0}\frac{V_0}{V_{1r}}\right|_{s=10} = \frac{0{\cdot}9k}{1 - 0{\cdot}4k^2/M_s^2}. \tag{41}$$

These relative amplitude ratios are plotted in Figure 1 as a function of k for the case $M_s = 10$. For $k > 1$, the relative density perturbation exceeds that in the radial velocity;

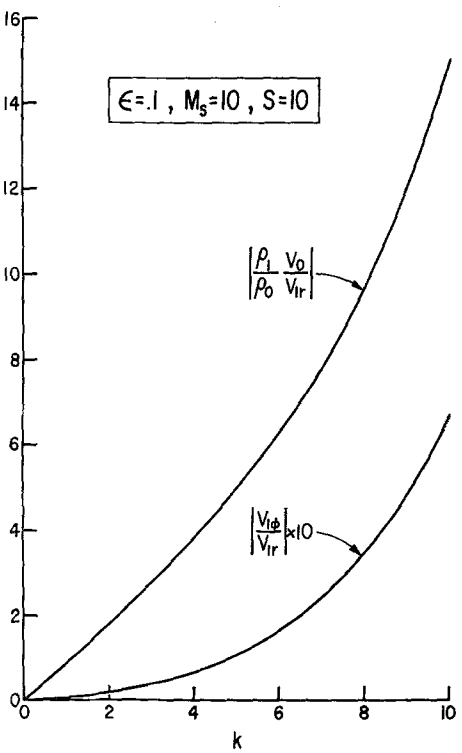

Fig. 1. Relative size of perturbations ϱ_1 and $V_{1\varphi}$ compared to V_{1r} as a function of k for $M_s = 10$, $\varepsilon = 0.1$, and $s = 10$.

however, $V_{1\varphi} < V_{1r}$ for all k. The relative size of ϱ_1 and $V_{1\varphi}$ compared with V_{1r} increases rapidly with k. If the mechanism under discussion produces a significant part of the observed variations in ϱ and V_φ, the k dependence should be revealed in power spectra of these quantities. The power density of the radial velocity, V_r, should fall off more rapidly with frequency than that of the density, ϱ, which in turn should fall off more rapidly than that of the azimuthal velocity, V_φ. This result is derived here for the low frequency range, $k < 10$, or for periods greater than $\frac{2}{1}\frac{5}{0} = 2.5$ days, and it might not apply to shorter period variations.

A physical interpretation of the result becomes clear when we look at the relative phases. Again ignoring the small imaginary part of x, if we choose the phase of $x(1)$ to be zero, we find for all s, phase$(x)=0$, phase$(y)=\pi$, and phase$(z)=-\pi/2$. With these we may consider the implied time sequence of measurements made at a fixed r and φ. This may be found from

$$V_{1r} = V_0 |x| \, e^{ik(\varepsilon s + \varphi)} \, e^{-ik\Omega t} \tag{42}$$

$$V_{1\varphi} = V_0 \frac{|y|}{s} e^{ik(\varepsilon s + \varphi)} \, e^{-i(k\Omega t - \pi)} \tag{43}$$

$$\varrho_1 = \varrho_0 |z| \, e^{ik(\varepsilon s + \varphi)} \, e^{-i(k\Omega t + \pi/2)} . \tag{44}$$

Thus, V_r and V_φ are anticorrelated and ϱ leads V_r by $\pi/2k\Omega$. The amplitude and phase relations for the case $k=4$ are shown in Figure 2 as a function of time for one period of the perturbation. The density reaches a maximum on the rising slope of V_r and a minimum on the downward slope which can be understood from the 'snowplow'

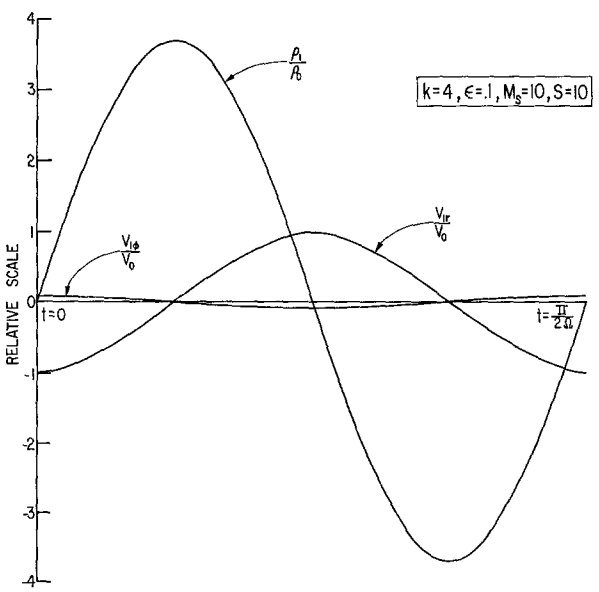

Fig. 2. Relative phases and amplitudes of the three perturbations for the case $k=4$, $\varepsilon=0.1$, $M_s=10$ and $s=10$.

model of stream interactions. The solar rotation is responsible for the spiral configuration of streams which causes fast streams to push against preceding slow ones. The pushing compresses the intervening gas causing a high density there. Similarly, the fast streams pull away from succeeding slow streams causing rarefaction of the intervening gas and a low density there.

The behavior of $V_{1\varphi}$ can also be understood in terms of this model. The figure shows that $V_{1\varphi}$ is maximum negative for V_{1r} maximum positive and vice versa. Thus, in the conventional astronomical sense of east and west (see Figure 3), fast streams flow from the west and slow streams from the east. This effect results from azimuthal stresses developed in the spiral interfaces between fast and slow streams as is shown schematically in Figure 3. The high pressure and low pressure regions result from the compression and rarefaction along the leading and trailing sides respectively of fast streams. The pressure gradient stresses have azimuthal components which in all cases accelerate the fast stream plasma toward the east and the slow stream plasma toward the west. There results the east–west asymmetry predicted by the theory.

In the above discussion the average of V_φ is zero whereas in reality it may be nonzero because of azimuthal viscous and magnetic stresses ignored here or because of the density–velocity correlation effect discussed by Siscoe *et al.* (1969a). The present result is therefore better stated as fast streams flow from the west and slow ones from the east with respect to the *average* azimuthal velocity.

4. Contact with Reality

The present theory applies to large scale rotating structures such as were seen during

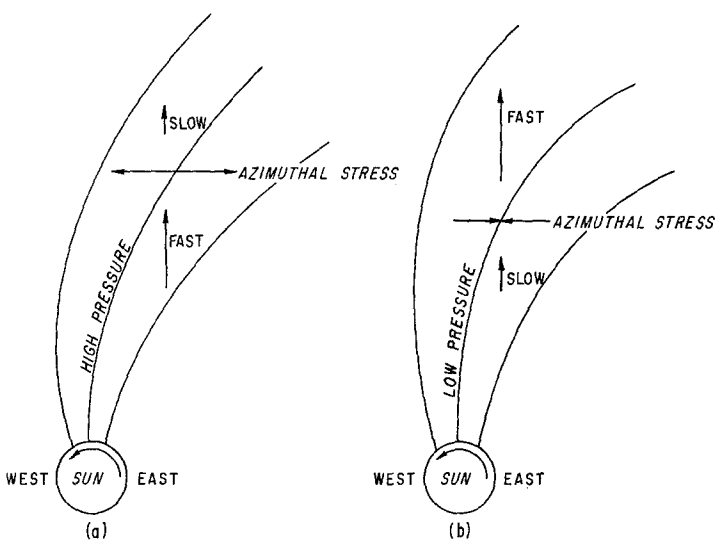

Fig. 3. A schematic representation of the interaction between fast and slow solar wind streams. (a) Slow stream preceding. (b) Fast stream preceding.

the declining phase of the last solar cycle by instruments on board Mariner 2, Mariner 4, and IMP1. We will consider the IMP1 observations first.

The well-known interplanetary sector structure was revealed through study of the IMP1 data (Wilcox and Ness, 1965). The structure observed was approximately corotating variations corresponding to the case $k=4$ in the solar wind speed and density and in the magnetic field. The average density and speed variations for one period (one sector) is shown schematically in Figure 4 which is taken from Wilcox and Ness (1967). The relationship between the two variables is similar to that in Figure 2, in that the density peaks on the rising slope of the speed and it reaches a minimum on the falling slope. Quantitatively the situation is represented approximately by $V_0=310$, $V_{r1}=30$, $\varrho_0=10$, and $\varrho_1=4$. Thus, $(\varrho_1/\varrho_0)(V_0/V_1)\approx 4$ which should be compared with the value 3.7 given by the theory. The agreement might appear fortuitous because we arbitrarily set the origin of the perturbation at $a=0.1$ AU. However, the theoretical value of the above ratio depends on a only in the combination $\varepsilon(s-1)=$ $=(\Omega/V_0)(r-a)$. The right hand side at 1 AU is very close to unity for any a small compared to 1 AU. Thus, the result is essentially independent of a.

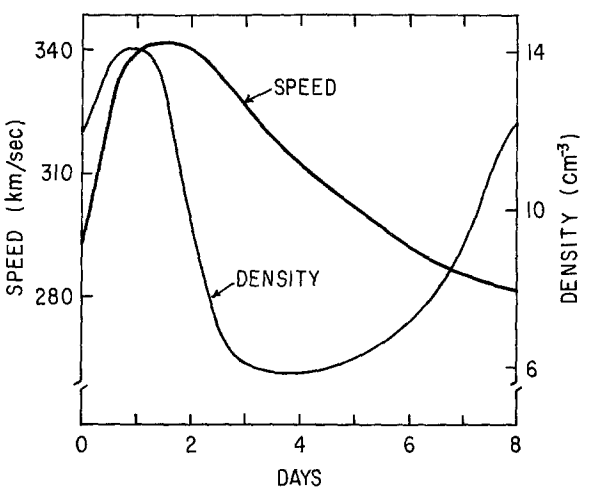

Fig. 4. A sketch of average behavior of the speed and density in a sector ($k=4$). From Wilcox and Ness (1967).

The behavior of V_φ seen by IMP1 is presently under study and will be reported in a subsequent article.

The density was observed to peak as the speed increased in both the Mariner 2 data (Neugebauer and Snyder, 1966) and the Mariner 4 data (Lazarus *et al.*, 1967). The magnetic field intensity was also observed to peak as the speed increased (Neugebauer and Snyder, 1967), and both effects were there interpreted as the results of compression. Although the magnetic field was omitted, its structure is easy to infer from the present calculation. The zero order field configuration consists of corotating

Archimedes' spirals. The effect of the radial velocity perturbation will be to compress the field at the leading edge of the fast stream and to rarefy it at the trailing edge as for the density. Thus, the expected density and magnetic profiles produced should be similar.

The direction of flow was not measured by either Mariner experiment. The predicted east–west asymmetry has been inferred from the observed asymmetry in the orientation of tangential discontinuities observed by Mariner 4 and Pioneer 6 (Siscoe *et al.*, 1969b), and it is now being studied directly with Pioneer 6 and 7 data. Other observations have shown that the solar wind direction deviates from the sun-spacecraft line frequently as much as 5° and occasionally as much as 10° (see, for example, Lyon *et al.*, 1968). We can calculate the deviation expected from the fast stream-slow stream interaction mechanism for a reasonable situation. Take $M_s=7$, $V_0=400$ km/sec, $V_{1r}=100$ km/sec, $k=4$, $\varepsilon=0.1$, and $s=10$. Then from equation (40), $V_{1\varphi}=14$ km/sec. In Appendix A, we show that for $\gamma=\frac{3}{2}$ (probably more realistic) this value is larger by about 50%. Therefore, we estimate $V_{1\varphi}\approx 20$ km/sec in this case. The angle of deviation is then approximately $\frac{20}{400}=\frac{1}{20}$ rad $\approx 3°$. It is possible that if the magnetic field were included, the effective Mach number would be smaller by about a factor of 2, and the angle estimate would double. However the calculation must be done before the effect of the magnetic field can be fully known.

Appendix A

THE CASE $\gamma=\frac{3}{2}$

This case comes closer to describing free adiabatic expansion for which $\gamma=\frac{5}{3}$ than the $\gamma=1$ case treated in the text and will indicate, thus, the sensitivity of the solutions to the choice of γ in the range of interest. For $\gamma=\frac{3}{2}$, the exact zero order solutions describing the solar wind expansion beyond the critical point can be taken to be

$$V_0 = \text{constant} \tag{A1}$$

$$\varrho_0 = \varrho_a \frac{a^2}{r^2} \tag{A2}$$

which were only approximate solutions in the previous case (Parker, 1963, p. 71). Since $c_s^2 \propto \varrho^{\gamma-1}$, the zero order sound speed now depends on distance through the relation

$$c_s^2 = c_a^2 \frac{a}{r} \tag{A3}$$

and also the Mach number

$$M_s^2 = \frac{V_0^2}{c_s^2} = M_a^2 \frac{r}{a}. \tag{A4}$$

With the x, y, z, s variables used earlier the φ-momentum equation, the 'Bernoulli'

equation and the continuity equation become, respectively

$$y' + \frac{ik}{M_a^2}\frac{z}{s} = 0 \tag{A5}$$

$$x - \varepsilon y + \frac{z}{M_a^2 s} = f \tag{A6}$$

$$x' + ik\varepsilon x + ik\frac{y}{s^2} + z' = 0. \tag{A7}$$

Eliminating x and z gives

$$(sM_a^2 - 1)\, y'' + (M_a^2 - 2ik\varepsilon)\, y' + k^2\left(\frac{1}{s^2} + \varepsilon^2\right) y = -k^2\varepsilon f \tag{A8}$$

which should be compared with Eq. (32) to notice the effect of changing γ.

As in the previous case, Eq. (A8) can be solved approximately for the boundary conditions

$$y(1) = z(1) = 0, \qquad x(1) \neq 0. \tag{A9}$$

If $M_s^2(s=10) = 100$, then $M_a^2 = 10$, also recall $k\varepsilon \leqslant 1$; hence approximately

$$sy'' + y' = -\frac{k^2\varepsilon f}{M_a^2}. \tag{A10}$$

The solution of (A10) satisfying (A9) is

$$y = -\left[(s-1) - \ln s\right]\frac{k^2\varepsilon}{M_a^2}x(1). \tag{A11}$$

From (A5) and (A6) we find

$$z = -ik\varepsilon(s-1)x(1) \tag{A12}$$

$$x = \left\{1 + \frac{ik\varepsilon}{M_a^2}\frac{s-1}{s} - \left[(s-1) - \ln s\right]\frac{k^2\varepsilon}{M_a^2}\right\}x(1). \tag{A13}$$

The phase relations revealed here are identical with those found in the previous case if we ignore the small imaginary part of x. The k dependence of the amplitudes is also very similar in the two cases. The radial dependence is essentially the same for the density but there is a difference in the azimuthal velocity growth. $V_{1\varphi}$ is greater for the $\gamma = \frac{3}{2}$ case. $V_{1\varphi}/V_{1r}$ is plotted for the two values of γ with $k=4$, $\varepsilon = 0.1$, $M_a^2 = 10$, $M_s^2 = 100$ in Figure 5. At $s=10$, $V_{1\varphi}(\gamma = \frac{3}{2})$ is about 50% larger than $V_{1\varphi}(\gamma = 1)$.

Appendix B

GENERAL BOUNDARY CONDITIONS

We wish to find an approximate solution to

$$(M_s^2 - 1)y'' - 2ik\varepsilon y' + k^2\left(\frac{1}{s^2} + \varepsilon^2\right)y = -k^2\varepsilon f \tag{B1}$$

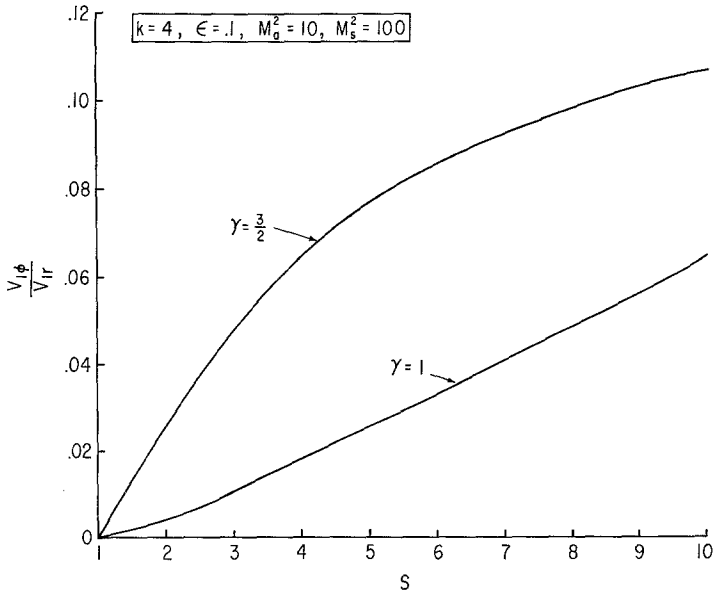

Fig. 5. The s dependence of $V_{1\varphi}/V_{1r}$ for $\gamma = 1$ and $\gamma = \frac{3}{2}$ in the case $k = 4$, $\varepsilon = 0.1$, $M_a^2 = 10$, $M_s^2 = 100$.

for arbitrary $y(1)$ and $y'(1)$, with $10 < M_s^2 < 100$, $k \leqslant 10$, and $\varepsilon \approx 0.1$. Hence, the second term of the left hand side can be neglected compared to the first. The third term is comparable to the first near $s = 1$, but gets smaller as s increases. Define the variable y_1 by

$$y = A + Bs + \frac{y_1}{M_s^2} \tag{B2}$$

where

$$B = y'(1), \qquad A = y(1) - y'(1). \tag{B3}$$

Then, the boundary condition on y_1 is

$$y_1(1) = y_1'(1) = 0. \tag{B4}$$

Thus, the third term will always be small in the equation for y_1, and we find that approximately

$$y_1'' = 2ik\varepsilon B - k^2\left(\frac{1}{s^2} + \varepsilon^2\right)(A + Bs) - k^2\varepsilon f. \tag{B5}$$

The solution of (B5) consistent with (B4) is

$$\begin{aligned} y_1 = {} & \tfrac{1}{2}(2ik\varepsilon B - k^2\varepsilon f - k^2\varepsilon^2 A^2)(s-1)^2 - \tfrac{2}{3}k^2\varepsilon^2 B(s-1)^2(s+2) \\ & - k^2 B(s\ln s - s + 1) - k^2 A(s - 1 - \ln s). \end{aligned} \tag{B6}$$

The restriction on the validity of (B6) is the same as the special case treated earlier.

Acknowledgements

This work was largely completed while the authors were at the Center for Space Research of the Massachusetts Institute of Technology and was supported by the National Aeronautics and Space Administration under grant NsG-386. This work was also partially supported by the Air Force Cambridge Research Laboratory, Department of Aerospace Research, under contracts AF 19(628)5543 and F 19628-69-C-0134.

References

Dessler, A. J.: 1967, *Rev. Geophys.* **5**, 1.
Lazarus, A. J., Bridge, H. S., Davis, J. M., and Snyder, C. W.: 1967, in *Space Res.* Vol. VII, North-Holland Publishing Co., Amsterdam.
Lyon, E., Egidi, A., Pizzella, G., Bridge, H., Binsack, J., Baker, R., and Butler, R.: 1968, in *Space Res.* Vol. VIII, North-Holland Publishing Co., Amsterdam.
Montgomery, M. D., Bame, A. J., and Hundhausen, A. J.: 1968, *J. Geophys. Res.* **73**, 4999.
Neugebauer, M. and Snyder, C. W.: 1966, *J. Geophys. Res.* **71**, 4469.
Neugebauer, M. and Snyder, C. W.: 1967, *J. Geophys. Res.* **72**, 1823.
Parker, E. N.: 1963, *Interplanetary Dynamical Processes*, Interscience Publishers, New York.
Parker, E. N.: 1965, *Space Sci. Rev.* **4**, 666.
Sarabhai, V.: 1963, *J. Geophys. Res.* **68**, 1555.
Siscoe, G. L., Goldstein, B., and Lazarus, A. J.: 1969a, submitted to *J. Geophys. Res.*
Siscoe, G. L., Turner, J. M., and Lazarus, A. J.: 1969b, *Solar Phys.* **6**, 456.
Strong, I. B., Asbridge, J. R., Bame, S. J., Heckman, H. H., and Hundhausen, A. J.: 1966, *Phys. Rev. Letters* **16**.
Wilcox, J. M. and Ness, N. F.: 1965, *J. Geophys. Res.* **70**, 5793.
Wilcox, J. M. and Ness, N. F.: 1967, *Solar Phys.* **1**, 437.